Journal of Nuclear Materials 528 (2020) 151843

Contents lists available at ScienceDirect

Journal of Nuclear Materials

journal homepage: www.elsevier.com/locate/jnucmat

Defect accumulation and evolution during prolonged irradiation of Fe and FeCr alloys

F. Granberg*, J. Byggmästar, K. Nordlund

Department of Physics, University of Helsinki, P.O. Box 43, FIN-00014, Finland

ARTICLE INFO

Article history:
Received 2 May 2019
Received in revised form
9 October 2019
Accepted 10 October 2019
Available online 15 October 2019

Keywords:
Irradiation
Molecular dynamics
Iron
Chromium
Alloy

ABSTRACT

The understanding of materials' behaviour during continuous irradiation is of great interest for utilizing materials in environments where harsh radiation is present, like nuclear power plants. Most power plants, both current and future ones, are based, at least partially, on Fe or FeCr alloys. In this study, we investigate the response of BCC Fe and several FeCr alloys to massively overlapping cascades. The effect of the added chromium on the defect accumulation and defect evolution was studied. Both a bulk setup, for observing the evolution deep inside the material far from grain boundaries and surfaces, and a setup with a nearby open surface, to investigate the effect of a permanent defect sink, were studied. We found that the primary defect production is similar in all materials, and also the build-up before serious overlap is comparable. When cascade overlap starts, we found that different sized clusters are formed in the different materials, depending on the setup. The defect cluster evolution was followed and could be related to the dislocation reactions in the materials. We found that the irradiation mixing was specific to the different chromium concentrations, the low chromium-containing alloy showed ordering, whereas the highest chromium-containing sample showed segregation.

1. Introduction

Iron and iron-chromium alloys are the base materials for many structural parts used in modern society. These materials are also the choice for constructing nuclear power plants, both in present and proposed concepts [1]. Some of the new proposed concepts are relying on higher temperatures, longer lifetimes and also higher doses of radiation, which places great demands on the material. It is known that the intensive radiation in these power plants will introduce defects, which ultimately will change the properties of the material. For instance, the mechanical properties of metals are known to be determined by the movement of dislocations. The mobility of dislocations are, on the other hand, dependent on the nanostructure of the material. Nanosized inclusions, voids, clusters, precipitates, impurities and defects will, at least to some degree, affect the movement of dislocations, for instance pin them and render them immobile [2–7]. The possible mixing and segregation of elements can also act to pin objects to mobile dislocations [8]. Immobile dislocations usually mean that the material becomes harder, but also more brittle, which can have detrimental effects on structural materials. This means that the nanosized defects, created and modified by irradiation, can ultimately affect the macroscopic behaviour of the material. Hence understanding their formation and evolution is important.

Irradiation experiments on Fe and FeCr alloys have shown that different defect structures are formed during irradiation. Both point defects and defect clusters can form, and these can then combine into even larger clusters. Vacancies can cluster and form voids and vacancy-type dislocation loops, and interstitials can combine and form C15-Laves phase clusters and interstitial-type dislocation loops. Two types of interstitial-type dislocation loops have been observed to form in iron and iron-based alloys, the $1/2\langle 111\rangle$ and the $\langle 100\rangle$ dislocation loops [9,10]. The $1/2\langle 111\rangle$ loop is mobile and can easily migrate, but the $\langle 100\rangle$ loop is immobile and can act as a defect sink. In irradiation experiments both types of loops have been observed [9,10], but the formation mechanism of the energetically less favourable loop, the $\langle 100\rangle$ loop, is yet not fully understood. At higher temperatures a transformation has been observed [11] and explained by anisotropic elasticity effects [12], but at lower temperatures the mechanism is still under debate, and several mechanisms have been suggested [13–19]. Hence, to understand the evolution of the properties of materials, it is of great

* Corresponding author.
E-mail address: fredric.granberg@helsinki.fi (F. Granberg).

https://doi.org/10.1016/j.jnucmat.2019.151843

interest to understand the formation of defects.

Most computational studies done on irradiation damage in materials are focused on the primary damage in single cascades [20]. These kinds of simulations give great insight in which kind of defects are produced, how many are produced and also the spatial separation of defect clusters, for instance as a function of recoil energy or irradiating particle [19,21–27]. Recently, some investigations have been carried out on the effect of cascade overlap with previous debris in Fe [18,28–31]. These studies showed that the number of defects produced is dependent on the pre-existing defect size and the separation distance [29], and also that existing dislocation loops can change the Burgers vector. There have been some investigations on the prolonged irradiation effects in metals done previously [32–35]. These studies are in some sense more comparable with experiments, as usually the doses achieved are much higher than what single cascades will achieve. These studies have shown that experimental doses, though at the low end, can be achieved by computer simulations. On one hand, the dose rates in these simulations are many order of magnitudes higher than in typical ion and neutron irradiation conditions (although similar dose rates can be achieved with plasma focused ion beam setups [36]). Hence in typical experiments, there may be significant point defect migration occurring between the cascades [37,38]. On the other hand, after rather moderate doses at room temperature, the defect structure is dominated by clusters (both in MD and rate theory [37,39,40]) which are usually immobile. After this situation is reached, the dose rate effects are likely to be less significant, and the MD simulations of defect cluster buildup may be at least qualitatively relevant for understanding also the damage evolution at lower dose rates. This argument is strengthened by the fact that previous MD simulations of damage buildup in metals have shown very good agreement with experiments [41]. Some prolonged irradiation studies have been conducted Fe and FeCr alloys previously [32,35]. One focused on elemental iron [35] and the previous study on Fe and FeCr alloys was done at a high energy and in a very small simulation cell [32], which will result in very frequent overlap of cascades with the pre-existing defects. The behaviour of chromium in FeCr alloys has been studied previously, where chromium atoms have been seen to diffuse and cause segregation [42–46]. MD simulations of damage overlap have also been done in semiconductors [47,48], insulators [49] and nanoclusters [50]. In all these cases very good agreement was obtained with experimental amorphization rates in spite of the high MD dose rate, because after the same damage overlap, most damage is in clusters and point defect migration is no longer important for the further evolution.

In this article, we focus on a larger cell and lower energy recoils to study the effect of prolonged irradiation of iron and iron-chromium alloys, with varying chromium contents. We focused on two different setups, a bulk setup to represent a sample deep inside the material far away from grain boundaries, and a setup with a nearby defect sink, in form of an open surface. All materials were subjected to 2 000 recoil events, resulting in a dose of 0.12 dpa. Several different aspects of the irradiation induced changes were studied. The number of point defects accumulated as a function of dose was investigated, and also the size distribution of the defect clusters. To study the possible segregation of chromium, the short range order and the detailed neighbourhood of chromium atoms were studied in all the alloys containing chromium. The interstitial-type defects were also analyzed for elemental segregation, as a function of cluster size. In addition to the cluster sizes, the created dislocation structures and their evolution were also investigated in all samples. These results, in form of size distributions and defect structures, can be used as input in higher scale models, like Discrete Dislocation Dynamics (DDD) [51–53].

2. Methods

All simulations were carried out with the classical MD code PARCAS [54,55], and the interatomic potential by Olsson et al. [56]. The interatomic potential is a two-band Embedded Atom Method (EAM) potential, describing the Fe and Cr interactions. Electronic stopping was used in all simulations, as a friction force on all atoms with a kinetic energy over 1 eV [57]. An adaptive timestep was utilized in all cascade simulations to accurately follow the trajectories of the energetic particles [58]. In this study, we investigated elemental Fe and five FeCr alloys with varying Cr content, all in a BCC structure. The FeCr alloys were to begin with random and the investigated Cr contents were 2.5 at-%, 5 at-%, 7.5 at-%, 10 at-% and 20 at-%. The simulations were carried out in two different setups, both a bulk and a surface setup. In the bulk setup, periodic boundary conditions (PBC) were applied in all directions to mimic an infinite single crystalline cell. In the surface setup, PBC were applied in two directions and a free surface was obtained by fixing a few layers of atoms at the bottom and leaving the boundary open at the top. In the bulk setup a simulation cell of $60 \times 63 \times 66$ unit cells was used, resulting in about 500 000 atoms. In the case of the surface setup, the same number of unit cells were used for the mobile atoms, and a few layers of fixed atoms were added to the bottom. To keep the temperature at 300 K, a Berendsen-type thermostat [59] was applied on all border atoms in the bulk setup and on a few layers of atoms above the fixed atoms in the surface setup.

To study the response of the materials to irradiation, 2 000 overlapping cascades of 5 keV each were simulated. The energy was given as kinetic energy to one Fe lattice atom, to mimic the energy transfer from an energetic particle to the primary knock-on atom (PKA) in the cell. In this setup, the accumulated dose is about 0.12 dpa [60], calculated with a displacement energy of 40 eV, which is the commonly used one for Fe and Fe-based alloys [61]. Each material was studied in three different separate runs, to obtain a more representative trend of the behaviour. The system was simulated for 30 ps after each initial recoil, to cool the system down to room temperature before the next recoil. To distribute the cascades homogeneously in the simulation cell, the recoil energy was given to one atom in the centre of the cell, in the bulk setup. This was done to hinder the cascade to interact with the thermally controlled layers of atoms. After each recoil, the simulation cell was shifted in all directions by a random amount. In the surface sample, the recoil energy was given to an atom in the middle third of the cell, to investigate the response of a bulk material with a nearby defect sink. This kind of simulation setup does not exactly correspond to any real irradiation condition, and hence this study is to be regarded as a model study of the effect of a nearby infinite planar defect sink on damage production. However, we do note that this model irradiation condition is actually not very far from an ion implantation with an energy that gives a damage maximum at the same depth (e.g. in the current case, SRIM simulations [62] show that 30 keV Ar ions under non-channeling conditions [63] would lead to a fairly similar recoil depth distribution). To homogeneously irradiate the cells in this setup, the simulation cells were shifted in both of the periodic $x-$, $y-$ directions by a random amount after each recoil. To analyze the number of defects produced in single recoil events in pristine materials, 100 single recoils were simulated in each material to obtain the average defect production without overlapping effects.

Wigner-Seitz analysis was performed to identify the point defects (vacancies and interstitials) [64]. To obtain the defect cluster statistics a cutoff between the 2nd and 3rd nearest neighbours was used for vacancies and between the 3rd and 4th nearest neighbours for interstitials. Wigner-Seitz analysis was used as it is one of the

few space-filling defect analysis methods. However, in rare cases, this method may yield the wrong defect structure and wrong number of defects close to complex defects, like the stacking fault tetrahedron in FCC [65]. To eliminate this possibility of wrong number of defects, the net balance of interstitials or vacancies in each cluster was determined in all cases. To furthermore study the exact structure of the defects, both C15-like structures and dislocation structures were determined. To obtain the chromium concentration in interstitial-type defects, we analyzed the atom types in multiply filled Wigner-Seitz cells. In the calculation of Short Range Order (SRO), varying cutoffs were used to investigate the SRO in different shells. All neighbours up to a certain cutoff and the neighbours in a certain interval were investigated. All numeric results given are the averages of the three different runs for each material, if not otherwise specified. The snapshots of the dislocation structure are taken from one of the three runs. To observe and analyze the dislocations in the samples, the Dislocation Extraction Algorithm (DXA) [66] implemented in OVITO [67] was used.

3. Results

All results presented in this section are the averages of the three different series conducted, if not otherwise indicated. There are some stochastic difference between the cases, which are visualized in the supplementary material (Suppl. Fig. 1). There the vacancy evolution as a function of dose is plotted for all three runs for some of the samples. The differences are small in the beginning, but in the end, mainly due to different dislocation structures, there are up to 5%–10% differences in the number of defects between the runs.

Results on all chromium contents will be described, however, only a few highlighted cases are shown as graphs in the main article for each of the different investigations. All graphical results are available for all samples in the Supplementary material found online.

3.1. Point defect accumulation

To study the accumulated defects in the different materials, we investigated the number of Wigner-Seitz defects [54] as a function of dose. In the case of the bulk investigation, we focused on the number of vacancies, which is the same as the number of interstitials and Frenkel pairs (FPs) (due to PBC). This point defect number calculation does not address the questions about the structure of the clusters, only the number of point defects in total. These questions related to ordering of point defects and structure of clusters are discussed later. In the investigation of the setup with a defect sink, we separated the vacancies and interstitials, as they have different migration barriers and can therefore reach the surface with different probabilities and rates. Another important factor is the number of adatoms, which is effectively the number of interstitials that have reached the surface reduced by the number of vacancies that reached the surface. Additionally, some vacancies and vacancy clusters were formed in the topmost layer of the cell, which are excluded from the total number of vacancies and vacancy cluster statistics, in similar manner as the adatoms are not included in the results for interstitials. The number of emitted atoms in the surface setup were the same in all investigated materials, and did therefore not show any dependence on the chromium content. This number was on the order of 50 after the 2000 initiated recoils.

To study the initial defect production, we also performed single impact simulations in all materials. The results of produced Frenkel pairs in a single 5 keV impact can be seen in Table 1.

In Fig. 1a, the number of vacancies is presented as a function of dose for all materials in the bulk setup. The alloys with a higher chromium content have started to saturate at a similar number of vacancies, whereas the low chromium content alloys still show a small increase in the number of retained vacancies. In the elemental Fe sample, on the other hand, the number of vacancies is still increasing linearly with dose.

Table 1
Number of Frenkel pairs produced by a single 5 keV cascade. The numbers are averages over 100 independent events. The error bars are the standard error of the mean.

Material	Number of FPs
Fe	11.2 ± 0.3
$Fe_{0.975}Cr_{0.025}$	11.0 ± 0.3
$Fe_{0.95}Cr_{0.05}$	10.5 ± 0.3
$Fe_{0.925}Cr_{0.075}$	11.3 ± 0.3
$Fe_{0.9}Cr_{0.1}$	11.7 ± 0.3
$Fe_{0.8}Cr_{0.2}$	12.1 ± 0.4

In Fig. 1b, the number of vacancies retained in the surface setup is presented for all materials. From the figure we can clearly see a different behaviour, compared to the bulk setup, Fig. 1a. Several general phenomena can be seen: 1) None of the materials have reached saturation; 2) The build-up rate is slower in the surface samples; 3) The alloy with highest chromium content shows the highest number of retained vacancies, in contrast to the bulk sample, and the elemental Fe sample shows similar number as the FeCr alloys, except the 20% chromium sample.

In Fig. 2a, the corresponding number of interstitials in the surface sample is presented. The graph clearly shows a difference between the behaviour of the materials. All materials have, except the 20% chromium sample, clearly reached a stable number of interstitials. The results show that the number of retained interstitials is corresponding to the chromium content, where a low or no chromium concentration will lead to a lower number of interstitials. In Fig. 2b, the number of adatoms is presented, which is closely related to the number of interstitials that have reached the surface. From this figure we can observe that the number of adatoms is highest in Fe and lowest in the 20% chromium sample. The other chromium alloys, that show similar a number of retained interstitials, show a similar number of adatoms. However, the order seems to be in the same order as the chromium content, where a higher concentration of Cr will yield a higher number of retained interstitials and a lower number of adatoms. The number of vacant atom positions in the surface layer, seen in Fig. 2c, is very similar in all materials, and increasing with dose.

3.2. Defect size distribution

The number of defects in different sized clusters in the bulk setup can be found in Fig. 3 and Fig. 4, for interstitial and vacancy clusters, respectively. The number of interstitials and vacancies in the surface setup can be found in Fig. 5 and Fig. 6, respectively. In these figures some representative cases are highlighted, and the same figures for other Cr concentrations can be found in the supplementary material online (Suppl. Figs. 2, 3, 6 and 7). The evolution of number of clusters can also be found for all materials in the supplementary material online.

In Fig. 3, the effect of chromium on the interstitial-type defect clusters can be seen in the bulk setup. A significant difference can be seen between the pure Fe sample and the samples containing chromium. Some differences can be seen in the number of interstitials in small interstitial clusters, but the main difference is seen for larger clusters (over ten defects per cluster). This is highlighted in Fig. 3c and Fig. 3d, where the number of interstitials in the two largest size intervals are shown for all chromium concentrations at two different doses. In pure Fe we do not see almost any

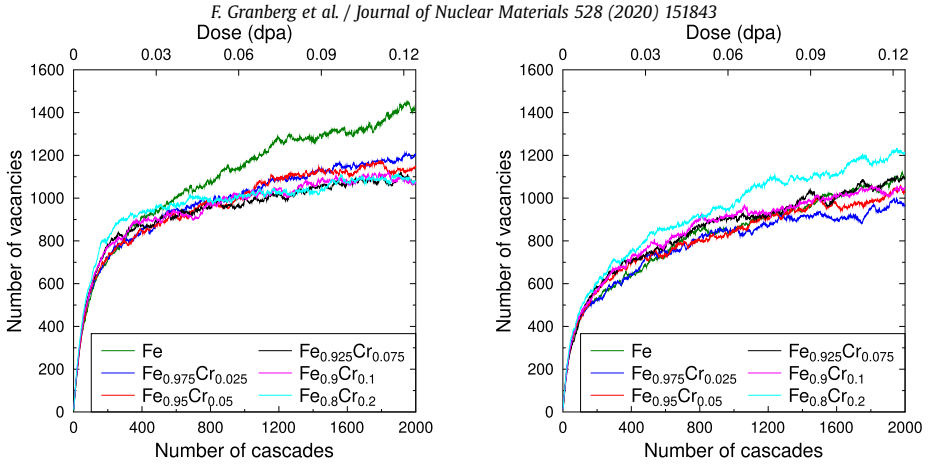

(a) Bulk (b) Surface

Fig. 1. Number of vacancies as a function of dose, in the bulk and surface setup.

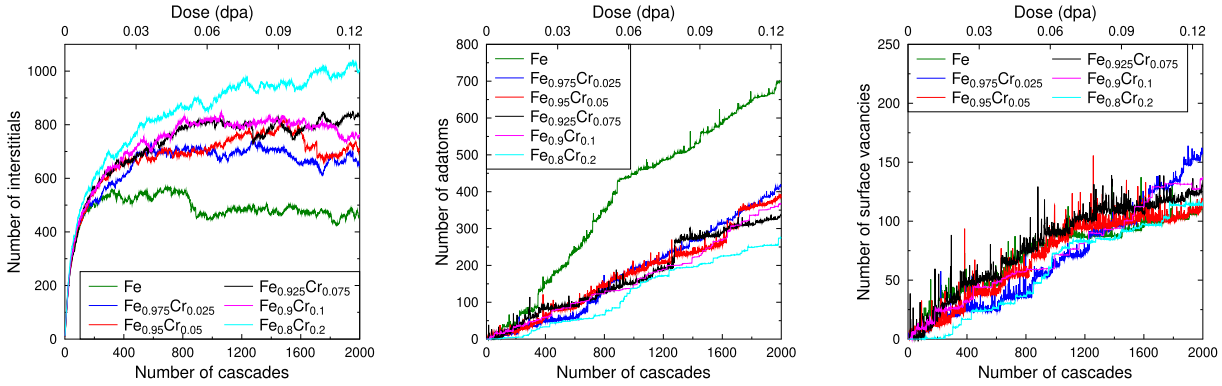

(a) Interstitials (b) Adatoms (c) Surface vacancies

Fig. 2. Number of interstitials, adatoms and vacant surface layer positions as a function of dose in the surface setup.

clusters in the range 10–50 defects when serious overlap has started, as most defects are in clusters larger than 50. In the chromium-containing samples we see, by increasing the chromium content, the number of defects in larger clusters is going down. In the 5% chromium sample there are still quite many defects in the largest clusters, but at 10% Cr and 20% Cr the numbers are very low. On the other hand, the number of defects in clusters of sizes 10 to 50 is higher in the high chromium-containing samples. The samples containing 2.5% and 7.5% chromium shows the same trend, and their response is between the pure Fe sample and the 5% sample and between the 5% sample and the 10% sample, respectively.

From the same figure, Fig. 3, the evolution of clusters can also be seen. For instance, for pure Fe, Fig. 3a, first we see a few single interstitials form, and also small clusters up to a few interstitials. After a while larger clusters start to form, and the number of defects in small clusters is decreasing. We also see that up to around 500 cascades, there are quite many defects in clusters of sizes 10 to 50, but as the dose increases, even larger clusters are formed and continue to grow. Similar general trends are seen for the chromium-containing samples. The huge differences are the times, e.g. number of cascades needed, for the larger clusters to start to form and the rate at which they are growing. The more chromium there is in the sample, the more cascades are needed for the larger clusters to form, and the slower they grow.

In Fig. 4, the number of vacancies in different sized vacancy clusters is plotted, as a function of dose for the bulk setup. The size intervals are different from the interstitial-type defects, as the vacancies do not cluster as much. The largest vacancy clusters, which rarely are observed, reach a maximum size of 40–50 vacancies in the bulk samples, however, for clarity all of these are all included in the 10+ interval. As seen in the total number of vacancies in these same samples, Fig. 1a, we see that the 20% chromium-containing sample show almost no increase in defect number after around 600 cascades, which is of course also seen here. We see that all sizes but the clusters larger than 10 vacancies are already saturated, and that the larger than 10 vacancy clusters are the reason for the slow increase in total number of vacancies. However, for pure Fe, we can observe that the number of vacancies in all sized clusters are increasing even at the end of the simulation run. The other high chromium concentration alloys, 7.5% and 10%, show a very similar trend as the 20% sample. The lower chromium concentration alloys, 2.5% and 5%, show an increase in all sized vacancy clusters, although their increase is less than that seen for pure Fe.

From Fig. 1b and Fig. 2a, we see that the number of vacancies are increasing in the surface sample for all chromium concentrations, but the overall number of interstitials have reached a saturation point for all samples except the 20% chromium sample. In Fig. 5, where the detailed cluster size analysis for interstitial clusters is shown, we can see that for pure Fe, all sized clusters have reached a steady state quite early in the simulation. On the other hand, for the 20% chromium sample, we see that the small interstitial clusters have reached saturation, but the larger clusters are still growing.

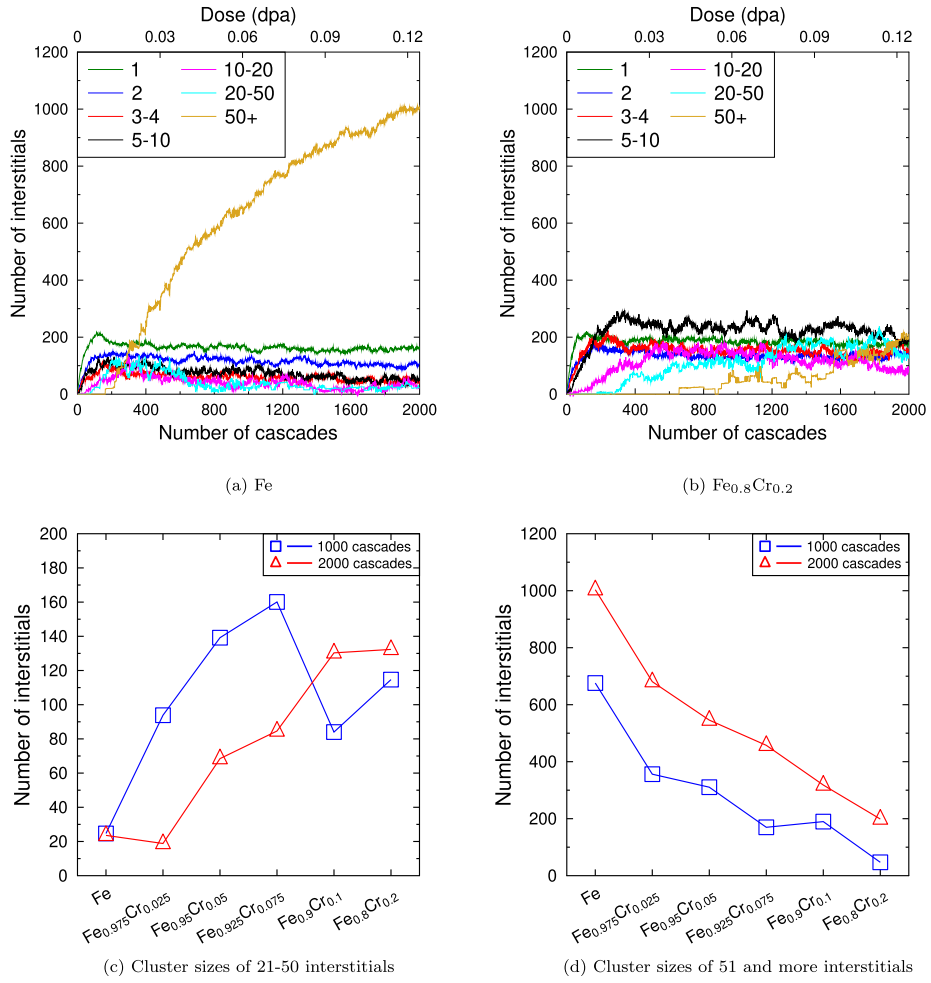

(a) Fe (b) $Fe_{0.8}Cr_{0.2}$

(c) Cluster sizes of 21-50 interstitials (d) Cluster sizes of 51 and more interstitials

Fig. 3. (a) and (b): Number of interstitials in different sized interstitial clusters for the bulk setup, for different chromium contents. The numbers are the average number of interstitials in the specific size interval. (c) and (d): Number of interstitials in large clusters as a function of chromium concentration, for two different doses. The values are the average over 20 frames.

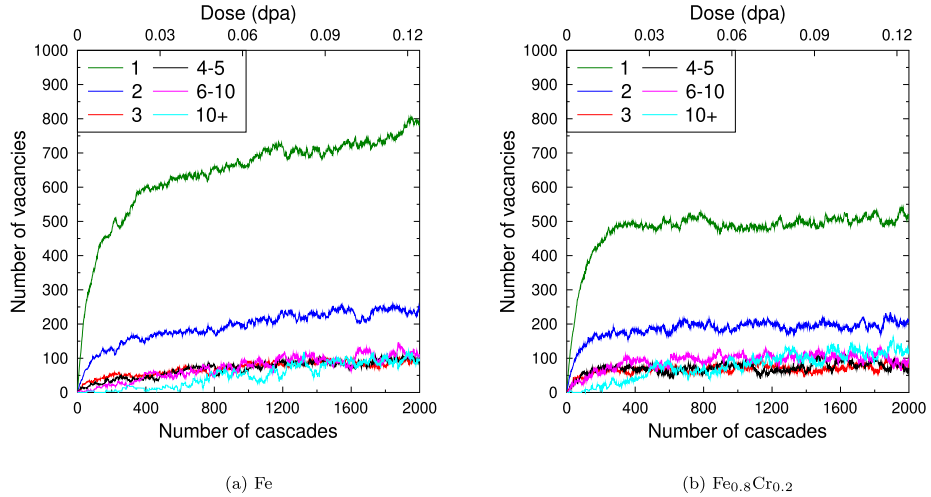

(a) Fe (b) $Fe_{0.8}Cr_{0.2}$

Fig. 4. Number of vacancies in different sized vacancy clusters for the bulk setup, for different chromium contents. The number is the average number of vacancies in the specific size interval.

The other chromium-containing alloys show on average that the number of defects in certain sized clusters have saturated, even though the fluctuations are higher in them compared to the pure Fe case.

For the vacancy clusters in the surface sample, we observe that the overall number is continuously increasing, and the reason can be seen in Fig. 6. In the surface setup, as larger vacancy clusters are formed compared to the bulk setup, an extra size interval is added.

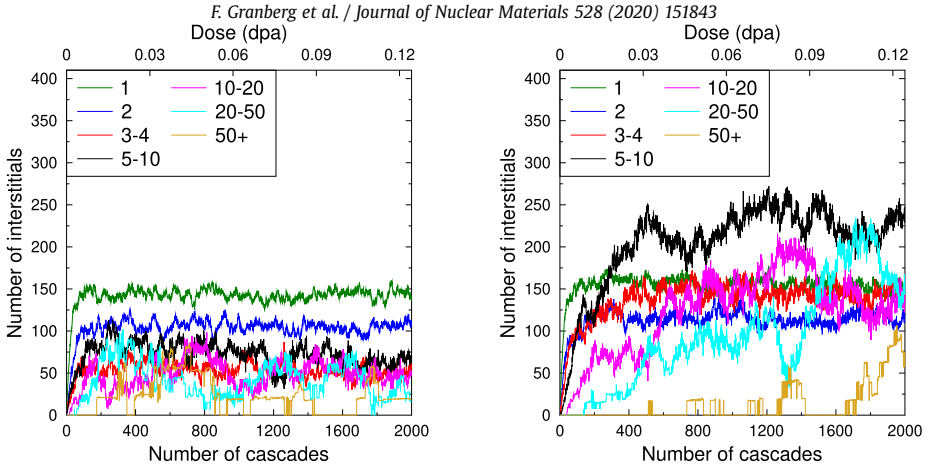

(a) Fe (b) $Fe_{0.8}Cr_{0.2}$

Fig. 5. Number of interstitials in different sized interstitial clusters for the surface setup, for different chromium contents. The number is the average number of interstitials in the specific size interval.

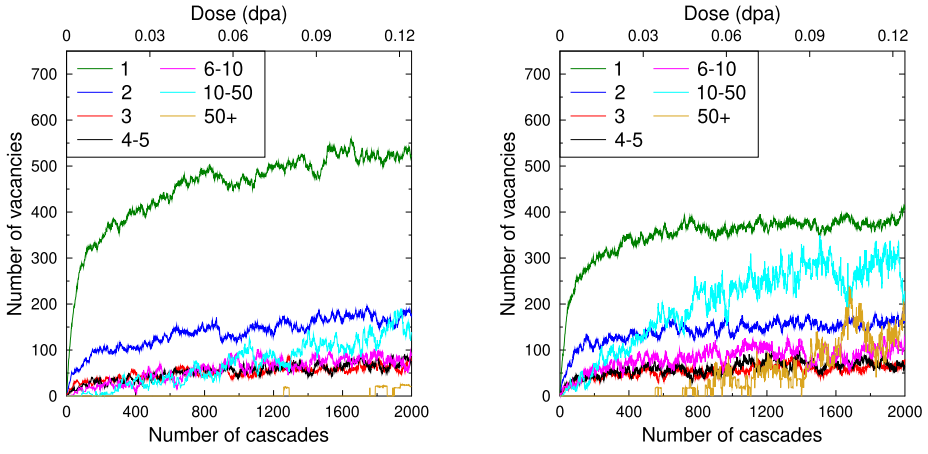

(a) Fe (b) $Fe_{0.8}Cr_{0.2}$

Fig. 6. Number of vacancies in different sized vacancy clusters for the surface setup, for different chromium contents. The number is the average number of vacancies in the specific size interval.

For the low chromium concentration samples (pure Fe, Fig. 6a), the amount of single vacancies is growing, and the larger clusters are growing in size and/or are increasing in number. For the high chromium concentration, (20% chromium, Fig. 6b), the large clusters are increasing more than in the lower chromium concentration samples. This leads to a higher overall number of vacancies in the 20% chromium-containing surface sample. This alloy also shows a larger increase in the large vacancy clusters compared to pure Fe and the other alloys.

The number of clusters of certain sizes can be found in the supplementary material online (Suppl. Figs. 4, 5, 8 and 9). These results are closely related to the presented amount of defects in certain sizes of defect clusters. These results can be used as input to higher scale models, to include the amount of differently sized clusters at a certain dose. However, as all trends needed for the conclusions can be seen for the previous results, these are not discussed in more detail in the main manuscript.

3.3. Defect structure and evolution

The evolution of dislocations for one of the three cases can be seen in the supplementary material online (Suppl. Figs. 10–13), for both the bulk and the surface setup. The frames are taken after 500, 1000 and 2000 initiated recoils in the different materials. The lines represents dislocation lines (green is 1/2⟨111⟩ and purple is ⟨100⟩) and the blue volumes are defective structures. These defective structure consists mainly of vacancy-rich disordered regions and some other small interstitial-type defects, like C15-Laves phase-type clusters. In elemental Fe we observe that there is a single large dislocation loop forming, whereas in the chromium-containing alloys we observe more but smaller dislocation loops. Both types of loops are seen, however, mainly the energetically more favourable 1/2⟨111⟩ loops. In the surface samples we do not observe as large dislocation structures as in the bulk sample, and also a depleted zone of defects close to the surface according to the DXA. The depth profile of defects can be found in the supplementary material online (Suppl. Figs. 14 and 15), where the profiles for both interstitials and vacancies for all material are found. In these graphs the depth profile of clusters consisting of five or more defects are also shown, to compare with the dislocation results.

Further analysis of the structure of the defects revealed that some of the interstitial-type clusters were in a C15-like structure. No drastic difference between the different chromium concentrations nor between the different setups were observed. The fractions of interstitials that were in a C15-like structure were around 1–6% after a few hundred cascades. The fluctuations are large, however,

the general trend is that whenever large dislocations are present, we observe fewer C15-like interstitials. This was observed as fewer C15-like interstitials in the bulk Fe and more in the 20% chromium-containing alloy in bulk. In the surface setup, most C15-like interstitials was observed in lower chromium-containing alloys and less in the higher chromium-containing alloys.

3.4. Short range order

The SRO evolution for the different chromium concentrations for both setups can be found in Fig. 7, where the first and second nearest neighbours are included. The SRO evolution for the other cutoffs can be found in the supplementary material (Suppl. Fig. 16). From the results we can see that in the beginning the samples were random, and that the irradiation will create ordering or segregation of chromium. From the figures we can for both setups observe ordering in the 2.5%–7.5% samples, a minute ordering in the 10% alloy, and segregation in the 20% alloy. Both setups show the same trends for this cutoff, and also for all the other investigated cutoffs. The absolute values are differing between the two setups a bit, and it is related to layers of atoms close to the surface, as well as the atom layers close to the fixed atoms. In the analysis, these layers are missing some of their neighbours, which of course affects the quantitative results. Therefore, in the results here, we focus on the bulk setup. All the results for also the surface can be found in the supplementary material online (Suppl. Figs. 16 and 17).

The SRO parameter for different shells in the alloys can be seen in Fig. 8. The different lines represent different included shells, the *upto* ones contains all neighbours up to a certain limit, for instance the *upto* 1NN includes only the first nearest neighbours and the *upto* 2NN both the first and second nearest neighbours and so on. The ones with *only* is only including the mentioned shell, not all atoms up to that shell. The 5% chromium alloy is illustrated in Fig. 8a and the 20% chromium alloy in Fig. 8b. From these figures we can observe that there are different effects happening in the different shells, which can explain the overall trend seen.

To study in more detail what is happening, we focus on the neighbourhood of chromium atoms. Here we study the number of chromium neighbours the chromium atoms have up to the 2NN shell. The alloys with 2.5%, 5% and 7.5% chromium all show the same trend. The fraction of chromium atoms with no chromium atoms as neighbours are increasing as a function of dose, whereas the chromium atoms with any amount of chromium atoms as neighbours are decreasing as a function of dose, see Fig. 9a for the 5% chromium sample. For the 10% chromium alloy, we observe minute changes in the neighbourhood, in line with the overall SRO change. In the 20% chromium-containing alloy we saw an overall segregation in the alloy, see Fig. 7. Looking into the neighbourhood of the chromium atoms we can observe a clear increase in chromium atoms with many chromium neighbours, see Fig. 9b.

3.5. Chromium concentration in defects

The chromium concentration in interstitial-type defect clusters are found in Fig. 10, for two samples in the bulk configuration. The results are the average over 50 frames in each run. Similar graphs for the other samples in both setups can be found in the supplementary material online (Suppl. Fig. 18). Both the bulk and the surface setups show similar fractions of Cr in the different sized interstitial clusters. For the lower chromium-containing alloys we can observe, especially in the smaller sized clusters, a higher fraction of chromium compared to the average chromium concentration, Fig. 10a. In the 10% chromium-containing alloy, only the single interstitials are chromium-rich, whereas the chromium concentration in the other clusters are the same as the ambient concentration. In the 20% chromium sample, Fig. 10b, we can observe a depletion of chromium compared to the ambient concentration, in all sized interstitial-type defect clusters.

4. Discussion

The single recoil simulations (Table 1) showed that the primary defect production in one cascade is not significantly affected by the amount of chromium content in the sample. A small difference was seen, where the 5% chromium alloy showed the smallest number of generated point defects and the 20% Cr alloy showed the highest number of defects. The difference is still not that significant that it can explain the differences in the accumulated defect numbers (seen in the next paragraph). These values are much smaller than the value predicted by NRT equation [60], $\sim$ 31 FPs, but very close to the more recent arcdpa value [68], $\sim$ 12 FPs, with the displacement energy of 40 eV and the constants for elemental iron. The similar defect production in all materials can also be seen as a similar amount of defects retained in all materials in the beginning of the overlapping cascades. The defect amount is increasing linearly in the beginning, where cascade overlap does not yet affect the

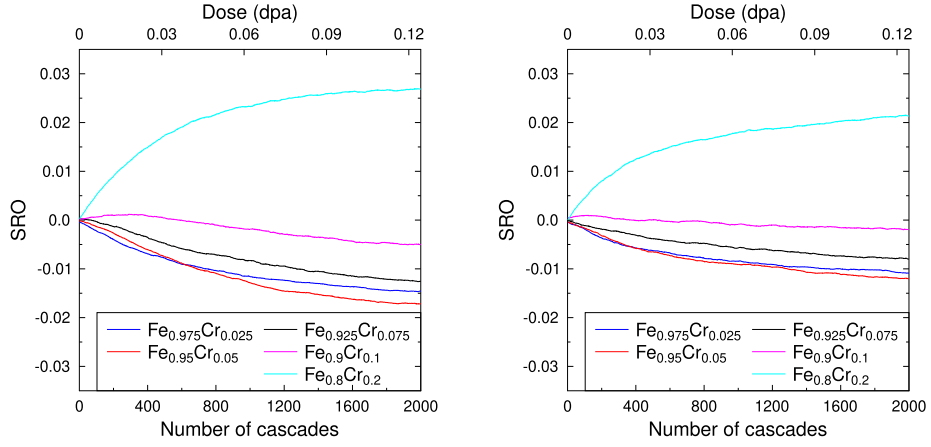

(a) Bulk setup

(b) Surface setup

Fig. 7. The SRO parameter for both setups for all chromium-containing alloys, where the atoms in the first and second nearest shells are included.

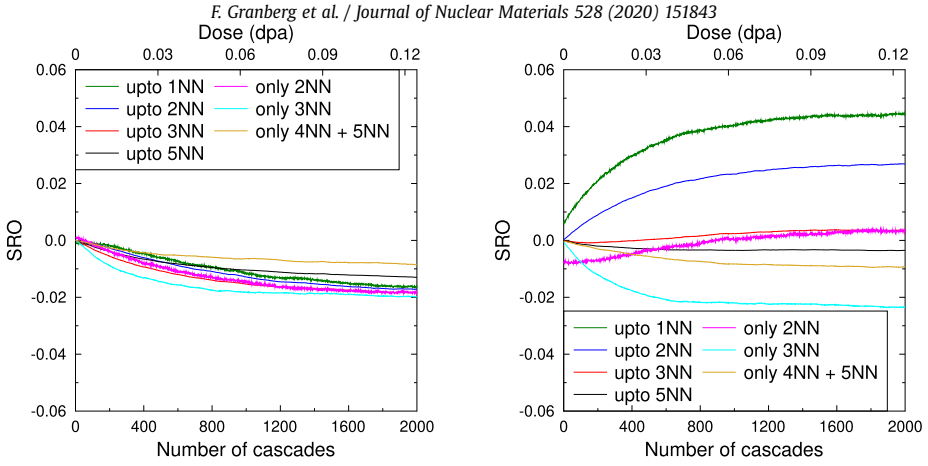

(a) $Fe_{0.95}Cr_{0.05}$ (b) $Fe_{0.8}Cr_{0.2}$

Fig. 8. The evolution of the SRO in different shells as a function of dose.

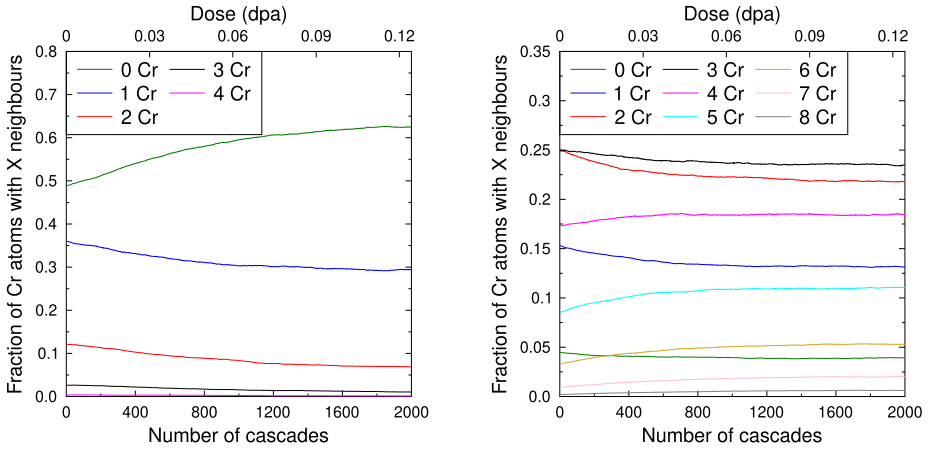

(a) $Fe_{0.95}Cr_{0.05}$ (b) $Fe_{0.8}Cr_{0.2}$

Fig. 9. Evolution of the detailed neighbourhood of chromium atoms.

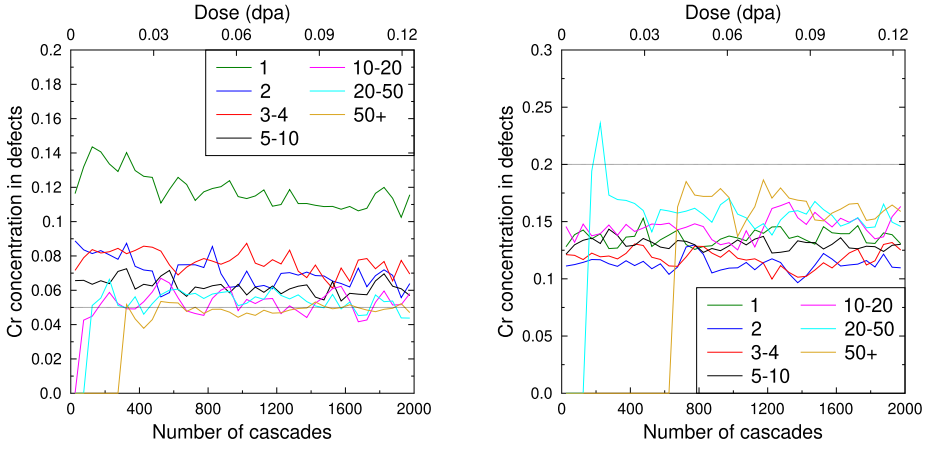

(a) $Fe_{0.95}Cr_{0.05}$ (b) $Fe_{0.8}Cr_{0.2}$

Fig. 10. Fraction of chromium atoms in interstitial-type defects of different sizes. The dashed line is the fraction of Cr in the sample.

results, and all samples are behaving similarly. After about 100 cascades, the different materials start to behave differently depending on the chromium content, and also the setup, bulk or surface, will affect the defect build-up drastically.

As the dose increases, we start to observe differences between the materials and setups for interstitials. We can see that the defects are mobile in elemental Fe and in the low chromium-containing alloys. This will in the bulk setup lead to larger defect

clusters, however, in the surface setup this will lead to the annihilation of some of the defects. This explains the opposite behaviour in the different setups for interstitials. The reason for the behaviour can be seen in the cluster size evolution of the different materials and setups. In elemental Fe we can see the fastest growth of intermediate interstitial clusters, which mainly are dislocation loops. These are usually mobile, which means that they can in the bulk setup combine and form even larger dislocations and dislocation networks. These large dislocations then absorb the nearby defects and keep growing. The chromium-containing samples also show a growth of defect clusters, however, the onset is at a higher dose and also the increase is slower. This can be observed to be due to the less mobile or immobile dislocation loops in the chromium-containing alloys. In especially the higher chromium-containing alloys, the dislocations are not mobile at all, leaving them relatively small, and having no recombination effects. Some movement can be seen from the heat and shock waves of nearby cascades. On one hand, cascades will introduce new defects to the material, which can be absorbed by the pre-existing defects. However, this is the case for all materials, except for the point defect diffusion rates, which are different. On the other hand, the mobile dislocations in Fe and low concentration Cr samples will move and absorb defects, which make them grow faster, which is related to the dislocation mobility in the samples. The reduced dislocation mobility in chromium-containing samples has been studied earlier in for instance Refs. [69] and [70]. In the surface sample, the mobile loops in the intermediate stage can reach the surface and annihilate in the low chromium-containing samples, whereas they are immobile in the high chromium-containing cells, and therefore keep growing slowly. The changes can be more drastic in the surface sample, as when a loop combines with the surface, tens or even hundreds of defects can immediately vanish from the system, compared to the bulk setup. The differences in dislocation and interstitial-type point defect mobilities can also be seen in the number of adatoms. In pure Fe and the low Cr-containing alloys, we can observe a lot of adatoms, whereas the high chromium-containing alloys show much less adatoms. The number of vacancies reaching the surface was not affected by the chromium content.

The vacancies, on the other hand, have a much higher migration barrier, which is seen as a not as drastic difference between the setups. However, as the interstitials and interstitial clusters are moving to the surface, we are left with a vacancy-rich volume in the surface sample. This can be observed as more clustering of the vacancies in the surface sample compared to the bulk sample. This is a result of the missing interstitials that have annihilated at the surfaces, leading to an excess of vacancies inside the material. From the size evolution of the vacancy clusters, we can see that mainly single defects and small clusters are forming in the beginning. As the dose increases we see the sizes and the number of the clusters starting to increase. In the end, where saturation on an overall vacancy point defect level is observed, we still can see some small changes in the size distributions. These results show that the overlap of cascades with pre-existing defects can change the defect structures. There have been some studies on the details of the effect of cascades overlapping with certain defects structures, i.e. Refs. [18,28–31]. The size and number distributions of the different clusters obtained here can be used as input in higher scale models, to get size distribution of defects at different doses, for instance in DDD simulations.

Looking at the dislocations in the bulk cells, we can confirm that the large interstitial clusters are dislocations, mainly mobile 1/2⟨111⟩ loops. We can also observe the formation of the immobile ⟨100⟩ interstitials loops, which has been studied in more detail previously in Ref. [18]. The simulations showed that in all materials, at some point during the irradiation, ⟨100⟩ loops are formed. However, mainly 1/2⟨111⟩ loops are formed, as they are energetically more favourable. Also in the surface sample, the largest interstitial clusters are dislocations, and they are mainly of 1/2⟨111⟩-type. The dislocations are smaller compared to the bulk, as in elemental Fe and in low chromium-containing alloys they are quite mobile and can annihilate at the surface.

Investigating the depth profile of defects in the surface setup, we can observe after prolonged irradiation a vacancy peak in the centre, where the cascades are initiated, and a two-peak distribution of interstitials, around the centre. At the recoil event, interstitials are pushed away from the cascade centre, leaving behind a vacancy-rich volume. When many of cascades are initiated in the middle of the cell, we are left with a vacancy-rich middle layer and with interstitial-rich layers on both sides. Looking at the zone close to the surface with very few defect clusters according to DXA, we can, however, still observe some defects in this region. These defects are mainly point defects and very small clusters, as seen in the depth profiles. Only in a few of the cases clusters of five or more defects are seen in the depth profile figures in this region. This explains the scarcity of dislocations and defective volumes in the DXA analysis close to the surface.

Detailed investigation of the defect structure revealed that C15-like clusters are formed in all samples in similar amounts, regardless of chromium content. The fraction of C15-like interstitials was, however, only on the level of a few percent. The low fraction can be explained by the stability of C15 in the used potential [71]. There were no major differences between the alloys, and the fluctuations were large, however, some phenomena could be seen. In the cases where large dislocations were present, fewer C15-like interstitials could be observed. These cases were elemental Fe and low Cr-containing alloys in bulk setup, and the high chromium-containing alloys in the surface setup. The large dislocations found in these samples can easily during interaction dissolve the existing C15-like clusters.

Looking at the SRO for the different chromium concentrations, we could observe ordering for the low chromium-containing alloys, almost no change for the 10% chromium sample and segregation for the 20% chromium sample. For the low chromium-containing alloys we can observe a decrease in the SRO parameter for all different nearest neighbour shells. This, of course, is portrayed in the overall decrease of SRO, e.g. ordering. For the 10% chromium alloy, we saw a slight ordering, and it can be seen that the value for the 1NN shell is constant, while a small ordering is seen for the other shells. For the highest chromium-containing alloy, a clear segregation was seen for the first and second nearest shell. Looking at the shell specific data, we can observe that there is a clear segregation in the 1NN shell and an ordering in the 3NN shell, while the 2NN is almost constant during the simulation. Checking the detailed neighbourhood of the chromium atoms in the samples, similar trends can be seen. For the 2.5%–7.5% chromium samples, we can see an increase of chromium atoms with zero chromium neighbours and a decrease of chromium atoms with any number of chromium neighbours. For the 10% chromium alloy, we observe a minute increase in Cr atoms with zero chromium neighbours, no change for those with 1 Cr neighbour, and a minute decrease in the ones with 2 or 3 chromium neighbours. This is in line with the overall slight ordering seen. In the 20% Cr alloy we saw an overall segregation in the alloy. Looking into the neighbourhood of the chromium atoms we can observe a decrease of Cr atoms with 0–3 chromium atoms as neighbours and an increase in the fraction of Cr atoms with 4 and more chromium atoms as neighbours. This increase of chromium atoms with many chromium neighbour explain the overall segregation seen.

Investigation of the elemental structure of the interstitial-type defects revealed that in most cases for the smaller clusters there

is an excess of chromium compared to the average chromium concentration. For the sample with 2.5% Cr atoms, we can see an excess of chromium in the defect clusters up to sizes of tens of interstitials. For the 5% Cr sample the clusters up to ten defects are chromium-rich. For the 7.5% and 10% samples only the single interstitials have more chromium than the average cell. In the 20% chromium sample we can see a depletion of chromium in all sizes of interstitial clusters. As the largest interstitial cluster are dislocations that are mobile, it is understandable that they move through the cell and therefore contain the average chromium concentration. The single ⟨110⟩ interstitial dumbbell is most energetically favourable as a mixed one, one chromium and one iron atom (−0.1 eV compared to the double Fe-dumbbell), in an otherwise elemental iron environment [56]. The double chromium dumbbell is, however, less energetically favourable than the double iron dumbbell (+0.4 eV). This can explain the results that we observe an excess of chromium in the smallest interstitial defect clusters at low chromium concentrations. To analyze the behaviour in the higher chromium-containing alloys, formation energy calculations of the dumbbells in 10% and 20% samples were conducted. At 10% chromium the double iron and the mixed dumbbell have the same energy, and the double chromium the highest formation energy (+0.3 eV). On the other hand, in the 20% Cr sample, we found that the double iron dumbbell is the most stable one, followed by the mixed dumbbell (+0.1 eV) and with the double chromium one highest in energy (+0.2 eV). This explains why we still observe an excess of chromium in small clusters in the 10% chromium sample, and why we see a reduction of chromium as interstitials in the 20% sample.

5. Conclusions

In this article, we have studied the effect of massively overlapping cascades in Fe and five FeCr alloys. The defect amount, cluster evolution and short range order were studied up to a dose of 0.12 dpa, both in a bulk and a surface setup. In the beginning where there was no or minute cascade overlap, the materials behaved similarly. As the dose increased, the different FeCr alloy samples started to show different defect evolution. The main factors were seen the to be the dislocation and defect reactions and behaviour. In the low chromium samples, the dislocations were mobile and could combine into large dislocation networks, whereas in the high chromium-containing samples, they were left immobile and smaller. In the setup with a defect sink, the high mobility of dislocation changed the evolution drastically, as now the dislocation could annihilate at the surface. Both types of dislocation loops, the 1/2⟨111⟩ loop and the ⟨100⟩ loop, were observed, however the 1/2⟨111⟩ loop more readily, as it is energetically more favourable. The low chromium-containing samples all showed ordering, which was also seen as an increase of chromium atoms that did not have any chromium neighbours. The 10% chromium sample showed a minute ordering, which was mainly attributed to a small increase of Cr atoms with no chromium neighbours. The 20% chromium sample showed an overall segregation, which was seen as a decrease of chromium atoms with few chromium neighbours and a huge increase of chromium atoms with many chromium neighbours. In all samples, except the highest Cr-containing one, an excess of chromium in interstitial-type defects could be observed. The excess of chromium in small interstitial defects could be explained by the relative stability of the different interstitial dumbbells. Depending on the average concentration, different sized clusters became chromium-rich. The defect size distribution results obtained can be used in higher scale models, like DDD, to mimic certain irradiation doses.

Data availability

The raw/processed data required to reproduce these findings cannot be shared at this time due to technical or time limitations.

Declaration of competing interest

The authors declare that they have no known competing financial interests or personal relationships that could have appeared to influence the work reported in this paper.

Acknowledgments

This research was partially funded by the Academy of Finland project SIRDAME (grant 259886). Computer time granted by the IT Center for Science, CSC, Finland and the Finnish Grid and Cloud Infrastructure (persistent identifier urn:nbn:fi:research-infras-2016072533) are gratefully acknowledged. This work has been carried out within the framework of the EUROfusion Consortium and has received funding from the Euratom research and training programme 2014–2018 and 2019–2020 under grant agreement No 633053. The views and opinions expressed herein do not necessarily reflect those of the European Commission.

Appendix A. Supplementary data

Supplementary data to this article can be found online at https://doi.org/10.1016/j.jnucmat.2019.151843.

References

[1] S.J. Zinkle, G.S. Was, Materials challenges in nuclear energy, Acta Mater. 61 (3) (2013) 735–758.
[2] Y.N. Osetsky, D.J. Bacon, V. Mohles, Atomic modelling of strengthening mechanisms due to voids and copper precipitates in α-iron, Philos. Mag. 83 (31 – 34) (2003) 3623–3641.
[3] S.M. Hafez Haghighat, J. Fikar, R. Schäublin, Effect of interatomic potential on the behavior of dislocation-defect interaction simulation in α-Fe, J. Nucl. Mater. 382 (2) (2008) 147–153.
[4] D. Terentyev, D.J. Bacon, Y.N. Osetsky, Interaction of an edge dislocation with voids in α-iron modelled with different interatomic potentials, J. Phys. Condens. Matter 20 (44) (2008) 445007.
[5] R. Schäublin, S.M. Hafez Haghighat, Molecular dynamics study of strengthening by nanometric void and Cr alloying in Fe, J. Nucl. Mater. 442 (1, Supplement 1) (2013) S643–S648.
[6] F. Granberg, D. Terentyev, K.O.E. Henriksson, F. Djurabekova, K. Nordlund, Interaction of dislocations with carbides in BCC Fe studied by molecular dynamics, Fusion Sci. Technol. 66 (1) (2014).
[7] F. Granberg, D. Terentyev, K. Nordlund, Interaction of dislocations with carbides in BCC Fe studied by molecular dynamics, J. Nucl. Mater. 460 (2015) 23–29.
[8] G. Bonny, D. Terentyev, L. Malerba, Interaction of screw and edge dislocations with chromium precipitates in ferritic iron: an atomistic study, J. Nucl. Mater. 416 (1) (2011) 70–74.
[9] B.C. Masters, Dislocation loops in irradiated iron, Philos. Mag. 11 (113) (1965) 881–893.
[10] Z. Yao, M.L. Jenkins, M. Hernández-Mayoral, M.A. Kirk, The temperature dependence of heavy-ion damage in iron: a microstructural transition at elevated temperatures, Philos. Mag. 90 (35–36) (2010) 4623–4634.
[11] K. Arakawa, M. Hatanaka, E. Kuramoto, K. Ono, H. Mori, Changes in the Burgers vector of perfect dislocation loops without contact with the external dislocations, Phys. Rev. Lett. 96 (2006) 125506.
[12] S.L. Dudarev, R. Bullough, P.M. Derlet, Effect of the α-γ phase transition on the stability of dislocation loops in bcc iron, Phys. Rev. Lett. 100 (2008) 135503.
[13] J. Marian, B.D. Wirth, J.M. Perlado, Mechanism of formation and growth of ⟨100⟩ interstitial loops in ferritic materials, Phys. Rev. Lett. 88 (2002), 255507.
[14] D. Terentyev, K. Vörtler, C. Björkas, K. Nordlund, L. Malerba, Primary radiation damage in bcc Fe and Fe–Cr crystals containing dislocation loops, J. Nucl. Mater. 417 (1) (2011) 1063–1066.
[15] L.K. Béland, Y.N. Osetsky, R.E. Stoller, H. Xu, Interstitial loop transformations in FeCr, J. Alloy. Comp. 640 (2015) 219–225.
[16] H. Xu, R.E. Stoller, Y.N. Osetsky, D. Terentyev, Solving the puzzle of ⟨100⟩interstitial loop formation in bcc iron, Phys. Rev. Lett. 110 (2013) 265503.
[17] Y. Zhang, X.-M. Bai, M.R. Tonks, S. Bulent Biner, Formation of prismatic loops from C15 Laves phase interstitial clusters in body-centered cubic iron, Scr. Mater. 98 (2015) 5–8.

[18] F. Granberg, J. Byggmästar, A.E. Sand, K. Nordlund, Cascade debris overlap mechanism of ⟨100⟩dislocation loop formation in Fe and FeCr, EPL (Europhys. Lett.) 119 (5) (2017) 56003.
[19] Q. Peng, F. Meng, Y. Yang, C. Lu, H. Deng, L. Wang, S. De, F. Gao, Shockwave generates ⟨100⟩dislocation loops in bcc iron, Nat. Commun. 9 (1) (2018) 4880.
[20] K. Nordlund, S.J. Zinkle, A.E. Sand, F. Granberg, R.S. Averback, R.E. Stoller, T. Suzudo, L. Malerba, F. Banhart, W.J. Weber, F. Willaime, S.L. Dudarev, D. Simeone, Primary radiation damage: a review of current understanding and models, J. Nucl. Mater. 512 (2018) 450–479.
[21] L. Malerba, D. Terentyev, P. Olsson, R. Chakarova, J. Wallenius, Molecular dynamics simulation of displacement cascades in Fe–Cr alloys, J. Nucl. Mater. 329–333 (2004) 1156–1160.
[22] L. Malerba, Molecular dynamics simulation of displacement cascades in α-Fe: a critical review, J. Nucl. Mater. 351 (1) (2006) 28–38.
[23] D.A. Terentyev, L. Malerba, R. Chakarova, K. Nordlund, P. Olsson, M. Rieth, J. Wallenius, Displacement cascades in Fe–Cr: a molecular dynamics study, J. Nucl. Mater. 349 (1) (2006) 119–132.
[24] C. Björkas, K. Nordlund, Comparative study of cascade damage in Fe simulated with recent potentials, Nucl. Instrum. Methods Phys. Res., Sect. B 259 (2) (2007) 853–860.
[25] K. Vörtler, C. Björkas, D. Terentyev, L. Malerba, K. Nordlund, The effect of Cr concentration on radiation damage in Fe–Cr alloys, J. Nucl. Mater. 382 (1) (2008) 24–30.
[26] E. Zarkadoula, S.L. Daraszewicz, D.M. Duffy, M.A. Seaton, I.T. Todorov, K. Nordlund, M.T. Dove, K. Trachenko, The nature of high-energy radiation damage in iron, J. Phys. Condens. Matter 25 (12) (2013) 125402.
[27] E. Zarkadoula, S.L. Daraszewicz, D.M. Duffy, M.A. Seaton, I.T. Todorov, K. Nordlund, M.T. Dove, K. Trachenko, Electronic effects in high-energy radiation damage in iron, J. Phys. Condens. Matter 26 (8) (2014), 085401.
[28] A.E. Sand, J. Byggmästar, A. Zitting, K. Nordlund, Defect structures and statistics in overlapping cascade damage in fusion-relevant bcc metals, J. Nucl. Mater. 511 (2018) 64–74.
[29] J. Byggmästar, F. Granberg, A.E. Sand, A. Pirttikoski, R. Alexander, M.-C. Marinica, K. Nordlund, Collision cascades overlapping with self-interstitial defect clusters in Fe and W, J. Phys. Condens. Matter 31 (2019) 245402.
[30] F. Granberg, J. Byggmästar, K. Nordlund, Cascade overlap with vacancy-type defects in Fe, Eur. Phys. J. B 92 (7) (2019) 146.
[31] X. Wang, N. Gao, Y. Wang, H. Liu, G. Shu, C. Li, B. Xu, W. Liu, Molecular dynamics study on the burgers vector transition of nanometric dislocation loops induced by cascade in bcc-iron, J. Nucl. Mater. 519 (2019) 322–331.
[32] K. Vörtler, N. Juslin, G. Bonny, L. Malerba, K. Nordlund, The effect of prolonged irradiation on defect production and ordering in Fe-Cr and Fe-Ni alloys, J. Phys. Condens. Matter 23 (2011) 355007.
[33] F. Granberg, K. Nordlund, M.W. Ullah, K. Jin, C. Lu, H. Bei, L.M. Wang, F. Djurabekova, W.J. Weber, Y. Zhang, Mechanism of radiation damage reduction in equiatomic multicomponent single phase alloys, Phys. Rev. Lett. 116 (2016) 135504.
[34] E. Levo, F. Granberg, C. Fridlund, K. Nordlund, F. Djurabekova, Radiation damage buildup and dislocation evolution in Ni and equiatomic multicomponent Ni-based alloys, J. Nucl. Mater. 490 (2017) 323–332.
[35] J. Byggmästar, F. Granberg, K. Nordlund, Effects of the short-range repulsive potential on cascade damage in iron, J. Nucl. Mater. 508 (2018) 530–539.
[36] S. Lee, S.H. Saw, Plasma focus ion beam fluence and flux - scaling with stored energy, Phys. Plasmas 19 (2012) 112703.
[37] Y. Katoh, R.E. Stoller, A. Kohyama, Rate theory investigation of influence of cascade cluster formation and solute trapping on point defect agglomeration and extended defect evolution, J. Nucl. Mater. 212 – 215 (1994) 179–185.
[38] J. Gan, G.S. Was, R.E. Stoller, Modeling of microstructure evolution in austenitic stainless steels irradiated under light water reactor condition, J. Nucl. Mater. 299 (2001) 53.
[39] H. Wiedersich, The effect of defect clusters formed in cascades on the sink strength of irradiated materials, Nucl. Instrum. Methods Phys. Res. B 59/60 (1991) 51–56.
[40] R.E. Stoller, S.I. Golubov, C. Domain, C.S. Becquart, Mean field rate theory and object kinetic Monte Carlo: a comparison of kinetic models, J. Nucl. Mater. 382 (2 – 3) (2008) 77–90.
[41] S. Zhang, K. Nordlund, F. Djurabekova, F. Granberg, Y. Zhang, T.S. Wang, Radiation damage buildup by athermal defect reactions in nickel and concentrated nickel alloys, Mater. Res. Lett. 5 (6) (2017) 433–439.
[42] X. He, W. Yang, Z. Qu, S. Fan, Effects of irradiation on chromium's behavior in ferritic/martensitic FeCr alloy, Front. Energy Power Eng. China 3 (2) (2009) 181–183.
[43] O. Senninger, F. Soisson, E. Martínez, M. Nastar, C.-C. Fu, Y. Bréchet, Modeling radiation induced segregation in iron–chromium alloys, Acta Mater. 103 (2016) 1–11.
[44] F. Soisson, T. Jourdan, Radiation-accelerated precipitation in Fe–Cr alloys, Acta Mater. 103 (2016) 870–881.
[45] R. Herschberg, C.-C. Fu, M. Nastar, F. Soisson, Atomistic modelling of the diffusion of C in FeCr alloys, Acta Mater. 165 (2019) 638–653.
[46] F. Soisson, E. Meslin, O. Tissot, Atomistic modeling of α'precipitation in Fe-Cr alloys under charged particles and neutron irradiations: effects of ballistic mixing and sink densities, J. Nucl. Mater. 508 (2018) 583–594.
[47] J. Nord, K. Nordlund, J. Keinonen, Amorphization mechanism and defect structures in ion beam amorphized Si, Ge and GaAs, Phys. Rev. B 65 (2002) 165329.
[48] J. Nord, K. Nordlund, J. Keinonen, A molecular dynamics study of damage accumulation in GaN during ion beam irradiation, Phys. Rev. B 68 (2003), 184104.
[49] S. Zhang, O.H. Pakarinen, M. Backholm, F. Djurabekova, K. Nordlund, J. Keinonen, T.S. Wang, Absence of single critical dose for the amorphization of quartz under ion irradiation, J. Phys. Condens. Matter 30 (1) (2018), 015403.
[50] M. Backman, F. Djurabekova, O.H. Pakarinen, K. Nordlund, L.L. Araujo, M.C. Ridgway, Amorphization of Ge and Si nanocrystals embedded in amorphous SiO2 by ion irradiation, Phys. Rev. B 80 (2009), 144109.
[51] T. Diaz de la Rubia, H.M. Zbib, T.A. Khraishi, B.D. Wirth, M. Victoria, M.J. Caturla, Multiscale modelling of plastic flow localization in irradiated materials, Nature 406 (2000) 871.
[52] A. Lehtinen, F. Granberg, L. Laurson, K. Nordlund, M.J. Alava, Multiscale modeling of dislocation-precipitate interactions in Fe: from molecular dynamics to discrete dislocations, Phys. Rev. E 93 (2016), 013309.
[53] A. Lehtinen, L. Laurson, F. Granberg, K. Nordlund, M.J. Alava, Effects of precipitates and dislocation loops on the yield stress of irradiated iron, Sci. Rep. 8 (1) (2018) 6914.
[54] K. Nordlund, M. Ghaly, R.S. Averback, M. Caturla, T. Diaz de la Rubia, J. Tarus, Defect production in collision cascades in elemental semiconductors and FCC metals, Phys. Rev. B 57 (13) (1998) 7556–7570.
[55] M. Ghaly, K. Nordlund, R.S. Averback, Molecular dynamics investigations of surface damage produced by keV self-bombardment of solids, Philos. Mag. A 79 (4) (1999) 795.
[56] P. Olsson, J. Wallenius, C. Domain, K. Nordlund, L. Malerba, Two-band modeling of α-prime phase formation in Fe-Cr, Phys. Rev. B 72 (2005) 214119.
[57] C. Björkas, K. Nordlund, Assessment of the relation between ion beam mixing, electron–phonon coupling and damage production in Fe, Nucl. Instrum. Methods Phys. Res., Sect. B 267 (10) (2009) 1830–1836.
[58] K. Nordlund, Molecular dynamics simulation of ion ranges in the 1-100 keV energy range, Comput. Mater. Sci. 3 (4) (1995) 448–456.
[59] H.J.C. Berendsen, J.P.M. Postma, W.F. van Gunsteren, A. DiNola, J.R. Haak, Molecular dynamics with coupling to external bath, J. Chem. Phys. 81 (8) (1984) 3684.
[60] M.J. Norgett, M.T. Robinson, I.M. Torrens, A proposed method of calculating displacement dose rates, Nucl. Eng. Des. 33 (1) (1975) 50–54.
[61] R.E. Stoller, M.B. Toloczko, G.S. Was, A.G. Certain, S. Dwaraknath, F.A. Garner, On the use of SRIM for computing radiation damage exposure, Nucl. Instrum. Methods Phys. Res., Sect. B 310 (2013) 75–80.
[62] J. F. Ziegler, SRIM-2013 software package, available online at: http://www.srim.org.
[63] K. Nordlund, F. Djurabekova, G. Hobler, Large fraction of crystal directions leads to ion channeling, Phys. Rev. B 94 (2016) 214109.
[64] K. Nordlund, M. Ghaly, R. Averback, Defect production in collision cascades in elemental semiconductors and fcc metals, Phys. Rev. B 57 (13) (1998) 7556–7570.
[65] K. Nordlund, F. Gao, Formation of stacking-fault tetrahedra in collision cascades, Appl. Phys. Lett. 74 (18) (1999) 2720–2722.
[66] A. Stukowski, V.V. Bulatov, A. Arsenlis, Automated identification and indexing of dislocations in crystal interfaces, Model. Simul. Mater. Sci. Eng. 20 (8) (2012), 085007.
[67] A. Stukowski, Visualization and analysis of atomistic simulation data with OVITO – the Open Visualization Tool, Model. Simul. Mater. Sci. Eng. 18 (1) (2010), 015012.
[68] K. Nordlund, S.J. Zinkle, A.E. Sand, F. Granberg, R.S. Averback, R. Stoller, T. Suzudo, L. Malerba, F. Banhart, W.J. Weber, F. Willaime, S.L. Dudarev, D. Simeone, Improving atomic displacement and replacement calculations with physically realistic damage models, Nat. Commun. 9 (1) (2018) 1084.
[69] D. Terentyev, G. Bonny, L. Malerba, Mobility of dislocations in thermal aged and irradiated Fe–Cr alloys, J. Nucl. Mater. 386–388 (2009) 257–260.
[70] S.M. Hafez Haghighat, D. Terentyev, R. Schäublin, Atomistic simulation of the influence of Cr on the mobility of the edge dislocation in Fe(Cr) alloys, J. Nucl. Mater. 417 (1) (2011) 1094–1097.
[71] M.-C. Marinica, F. Willaime, J.-P. Crocombette, Irradiation-induced formation of nanocrystallites witves phase structure in bcc iron, Phys. Rev. Lett. 108 (2012), 025501.